Elastic origin of chiral selection in DNA wrapping

Tomohiro Yanao[1] and Kenichi Yoshikawa[1,2,3,*]
[1]*Fukui Institute for Fundamental Chemistry, Kyoto University, Kyoto 606-8103, Japan*
[2]*Department of Physics, Graduate School of Science, Kyoto University, Kyoto 606-8502, Japan*
[3]*Spatio-Temporal Order Project, ICORP, JST, Japan*
(Received 8 November 2007; published 6 February 2008)

We investigated the mechanism that underlies the chiral selection on the direction of wrapping of DNA around a nucleosome core particle. A coarse-grained model for the formation of a nucleosome is introduced, in which DNA is treated as a semiflexible polymer and the histone core is modeled by a spherical particle. Asymmetric coupling between bending and twisting is incorporated into the model DNA, which is expected from the double-stranded helical structure of DNA. We show that the tendency of DNA to twist in a left-handed manner upon bending gives rise to the selective left-handed wrapping, provided that the size of the core particle is chosen appropriately. This result suggests the critical importance of the chiral asymmetry inherent in the bending-twisting elasticity of DNA as well as the size of the core in determining the handedness of wrapping in nucleosome formation.

DOI: 10.1103/PhysRevE.77.021904 PACS number(s): 87.14.G−, 87.16.Sr, 87.15.H−

I. INTRODUCTION

Eukaryotic DNA is compactly stored in a tiny cell nucleus by assuming a highly organized and hierarchical structure, which is called chromatin [1,2]. The structure and dynamics of chromatin are essential for fundamental functions of DNA, such as transcription, replication, and duplication under the actions of various proteins and enzymes [3,4]. Therefore, it has been and is an important challenge to elucidate the structure as well as the mechanism of the formation of chromatin. The most elementary repeating unit of chromatin is the nucleosome [5], in which DNA is wrapped around a core particle (histone octamer) about 1.75 times in a left-handed manner. Therefore, understanding the stability and dynamics of the nucleosome is an important first step that could lead to elucidation of the higher-order functions of chromatin.

One of the most striking aspects of the nucleosome structure is the uniformity of the direction of wrapping (wrapping chirality). In particular, DNA is wrapped around the nucleosome core particle exclusively *in a left-handed manner* in nature. It would be very interesting to explore the origin of this chiral selection from the viewpoint of the intrinsic elasticity of DNA. The elasticity of DNA has been extensively investigated through, for example, mechanical stretching experiments [6,7]. It is well known that DNA is a relatively stiff polymer (semiflexible polymer) that can be modeled as a wormlike chain as a first approximation [8,9]. This semiflexible nature makes the coil-globule transition of long DNA molecules of more than several tens of kilobase pairs markedly discrete (first-order transition [10]) at the single-molecule level [11–13]. On the other hand, to understand the higher-order functions of DNA, such as supercoil formation [14–16], wrapping around core proteins [17–19], and chromatin dynamics [20], it is highly important to examine more detailed elastic properties of DNA.

The importance of the twisting elasticity of DNA in its functions can be naturally understood by noting the double-stranded helical structure of DNA. This helical structure implies that stretching as well as bending of DNA can couple with twisting in a characteristic manner. Coupling between stretching and twisting has been studied in detail both experimentally [21–23] and theoretically [24,25]. Recently, Besteman *et al.* [23] showed that an externally imposed twist on a DNA molecule can significantly affect its condensation transition under tension using the magnetic tweezers technique. Their result clearly shows the importance of coupling between stretching and twisting in DNA condensation. Coupling between bending and twisting has also been investigated [26–28] by taking into consideration the double-stranded helix structure of DNA. Marko and Siggia [26] showed that coupling between bending and twisting causes unwinding of the helix upon bending, i.e., the coupling is highly asymmetric. Such a kind of coupling between bending and twisting of DNA is expected to play an important role in the selection of the direction of wrapping in nucleosome formation. Recently, Tolstorukov *et al.* [29] gave a qualitative explanation for the selection of the direction of the wrapping by taking into consideration the asymmetric deformations of the duplex structure of DNA in great detail. In this paper, we present dynamical evidence that the asymmetric coupling between bending and twisting of DNA gives rise to the selection of the direction of wrapping by using the Langevin dynamics at the coarse-grained level.

In addition to the elastic properties of DNA, the geometric properties of the core particle should be of complementary importance in nucleosome formation. Recently, Zinchenko *et al.* [30,31] investigated the compaction of DNA by histone-inspired spherical particles and found that the manner of compaction changes markedly depending on the size of the particles. This result clearly indicates that the size of the core particles is an important parameter in the compaction (wrapping) of DNA. Meanwhile, Hamiche *et al.* [32] and Li *et al.* [33] suggested that the handedness embedded in the microscopic structure of the core particle influences the direction of wrapping of DNA around the core. However, since the

*yoshikaw@scphys.kyoto-u.ac.jp

core particle is generally under extensive thermal noise in an aqueous environment, the chirality in the core particle alone may not sufficiently secure the uniformity of the wrapping direction of DNA. Therefore, in the present study, we sought another complementary factor that may influence proper chiral selection in the wrapping—that is, the intrinsic chirality in the bending-twisting elasticity of DNA.

In this paper, we first introduce a coarse-grained model for the formation of a nucleosome by extending the homopolymer model proposed by Sakaue and co-workers [17,18]. Chirality, or asymmetry, is incorporated into the coupling between bending and twisting of our model DNA. We specifically assume that the dihedral angles of the model DNA has a tendency to shift (twist) in a left-handed direction when the backbone of DNA is bent. This property is expected from the right-handed nature of the double-stranded helical structure of DNA. The core particle, on the other hand, is modeled by an isotropic sphere and has no chirality. We show that the asymmetric coupling between bending and twisting of the model DNA gives rise to the selective left-handed wrapping with very high probability, provided that the size of the core particle is chosen appropriately. Although the electrostatic properties of DNA, the core, and the aqueous environment [2,34–37] may also be important in nucleosome formation in the real world, they are simply incorporated into a small number of parameters in our coarse-grained model since the main focus of the present study is the role of DNA elasticity and the size of the core particle.

This paper is organized as follows. In Sec. II, we introduce a coarse-grained model for a nucleosome that consists of a DNA-like semiflexible polymer and a histonelike core particle. Asymmetric coupling between bending and twisting of the polymer is highlighted. We then investigate the mechanism for the chiral selection in the wrapping of DNA around a core particle based on the Langevin dynamics in Sec. III. Our results show that the direction of wrapping of DNA can be determined by the asymmetric coupling between bending and twisting of DNA and by the size of the core particle. We conclude this paper with some remarks regarding future studies in Sec. IV.

II. COARSE-GRAINED MODEL FOR NUCLEOSOME FORMATION

A. Potential functions for bonding, self-avoiding, and the core particle

We introduce here a coarse-grained model for the formation of a nucleosome that consists of a DNA molecule and a histone core particle. DNA is modeled by a semiflexible homopolymer composed of n monomeric units that are successively connected by springs, while the histone core is modeled by a spherical particle. The number of constituent monomeric units of the homopolymer is set to $n=30$ throughout this study. The potential function of the whole system consists of four parts:

$$V = V_{\mathrm{bond}} + V_{\mathrm{avoid}} + V_{\mathrm{bend,twist}} + V_{\mathrm{core}}. \tag{1}$$

The first term V_{bond} is for the bonding between two adjacent monomeric units. The term V_{avoid} represents the self-avoiding effect of the polymer. The term $V_{\mathrm{bend,twist}}$ incorporates coupling between bending and twisting of DNA into the model. The term V_{core} is for the interaction between the core particle and DNA. The three terms V_{bond}, V_{avoid}, and V_{core} are introduced in this subsection based on the original model proposed by Sakaue and co-workers [17,18]. The potential function $V_{\mathrm{bend,twist}}$ is introduced in the next subsection.

A harmonic potential is used for the bonding between two neighboring monomeric units of the polymer:

$$V_{\mathrm{bond}} = \frac{\varepsilon}{2\sigma^2}\sum_{i=1}^{n-1} k_{\mathrm{bond}}(|\boldsymbol{b}_i| - \sigma)^2, \tag{2}$$

where ε is the unit of energy, $\boldsymbol{b}_i$ is the bond vector connecting monomer i and monomer $i+1$,

$$\boldsymbol{b}_i \equiv \boldsymbol{r}_{i+1} - \boldsymbol{r}_i \quad (i = 1, \ldots, n-1), \tag{3}$$

where $\boldsymbol{r}_i$ is the three-dimensional vector representing the position of the ith monomeric unit, and σ is the equilibrium distance between two adjacent beads. The dimensionless parameter k_{bond} in Eq. (2) represents the spring constant for bonding, which is set to $k_{\mathrm{bond}}=400$ so that the bond length $|b_i|$ is kept close to the constant σ during the conformational transition ($b_i \simeq \sigma$). In our model, the equilibrium bond length σ corresponds to about 2.9 nm, and the total length of the model polymer is thereby about 84 nm, which corresponds to a DNA molecule of about 250 base pairs. In the following, we set the parameters in the potential functions so that the model is consistent with this length scale.

The self-avoiding effect of DNA is modeled by the repulsive term of the Morse potential:

$$V_{\mathrm{avoid}} = \varepsilon_m \sum_{i=1}^{n-2}\sum_{j=i+2}^{n} \exp\{-\alpha_m(r_{ij} - \sigma_m)\}, \tag{4}$$

where $r_{ij} \equiv |\boldsymbol{r}_j - \boldsymbol{r}_i|$ is the distance between beads i and j. The parameters ε_m and α_m, which determine the strength and steepness of the repulsion between two nonadjacent monomeric units of the polymer, are set to $\varepsilon_m=0.2\varepsilon$ and $\alpha_m=24$, respectively, based on Ref. [17]. The parameter σ_m determines the repulsion distance between two nonadjacent monomeric units and is set to $\sigma_m=0.7\sigma$. With these settings, the radius of the model polymer can be regarded to be approximately $\sigma_m/2=0.35\sigma$, which corresponds to about 1 nm, the radius of the actual double-stranded DNA.

The interaction between the negatively charged DNA and the positively charged histone core is modeled by the Morse potential for simplicity:

$$V_{\mathrm{core}} = \varepsilon_{\mathrm{c}}\sum_{i=1}^{n} [\exp\{-2\alpha_{\mathrm{c}}(|\boldsymbol{r}_i - \boldsymbol{r}_{\mathrm{c}}| - \sigma_{\mathrm{c}})\} - 2\exp\{-\alpha_{\mathrm{c}}(|\boldsymbol{r}_i - \boldsymbol{r}_{\mathrm{c}}| - \sigma_{\mathrm{c}})\}], \tag{5}$$

where $\boldsymbol{r}_{\mathrm{c}}$ is the position vector that represents the center of the core. The parameter ε_{c}, which determines the strength of the interaction between the core particle and each monomeric unit of the polymer, is set to $\varepsilon_{\mathrm{c}}=7\varepsilon$. The parameter α_{c} represents the "width" of the pairwise Morse potential and is set to $\alpha_{\mathrm{c}}=6$. The parameter σ_{c} corresponds to the equilibrium

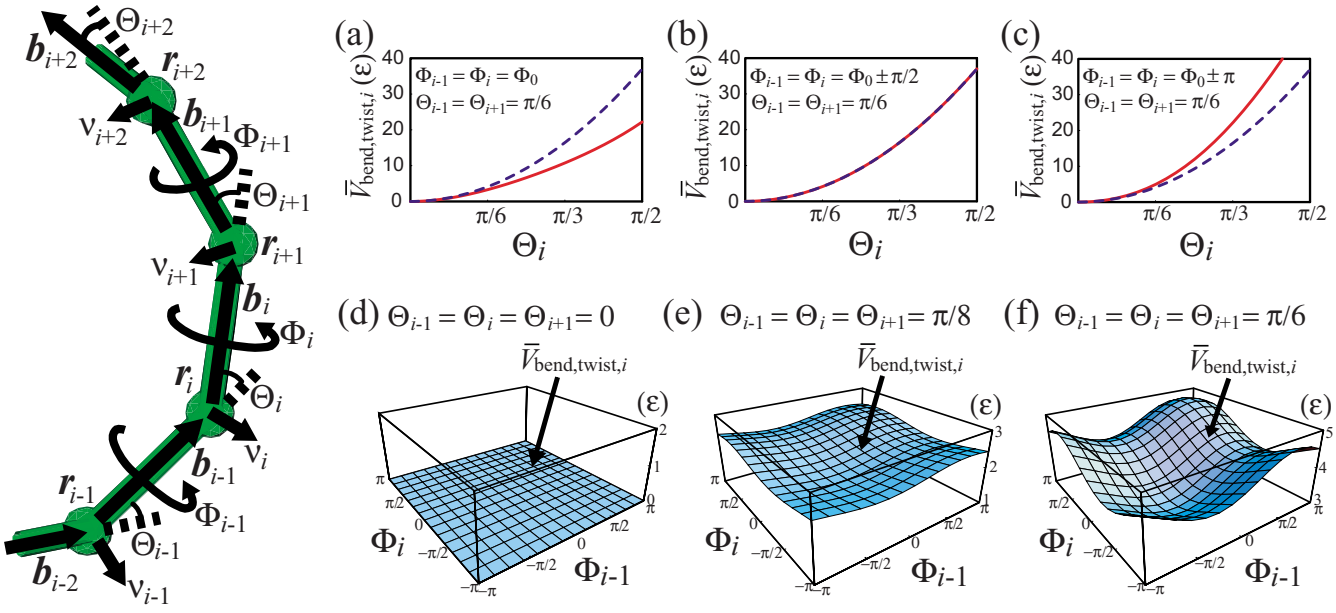

FIG. 1. (Color online) (Left) A schematic picture showing the definitions of the position vectors $\{\boldsymbol{r}_i\}$ of monomeric units, the bond vectors $\{\boldsymbol{b}_i\}$, the bending vectors $\{\boldsymbol{\nu}_i\}$, the bending angles $\{\Theta_i\}$, and the dihedral angles $\{\Phi_i\}$. (a)–(c) Dependence of the potential function $\bar{V}_{\mathrm{bend,twist},i}$ (units of ϵ) [Eq. (16)] on the bending angle Θ_i is shown with solid curves with other angle variables fixed at $\Theta_{i-1}=\Theta_{i+1}=\pi/6$ and $\Phi_{i-1}=\Phi_i=\Phi_0$ [in (a)], $\Phi_{i-1}=\Phi_i=\Phi_0\pm\pi/2$ [in (b)], and $\Phi_{i-1}=\Phi_i=\Phi_0\pm\pi$ [in (c)], respectively. For comparison, the harmonic potential $(\varepsilon/2)\kappa_0\Theta_i^2$ is also plotted with dashed curves in (a)–(c). (d)–(f) The potential function $\bar{V}_{\mathrm{bend,twist},i}$ is plotted as a function of the dihedral angles Φ_{i-1} and Φ_i with the bending angles fixed at $\Theta_{i-1}=\Theta_i=\Theta_{i+1}=0$ [in (d)], $\Theta_{i-1}=\Theta_i=\Theta_{i+1}=\pi/8$ [in (e)], and $\Theta_{i-1}=\Theta_i=\Theta_{i+1}=\pi/6$ [in (f)]. In all of these figures, the bending spring constants are set to $\kappa_0=30$ and $\kappa_{\mathrm{bt}}=12$, and the equilibrium dihedral angle is set to $\Phi_0=-\pi/3$.

distance between the center of the core and that of a monomeric unit. Since the radius of the polymer is considered to be $\sigma_m/2=0.35\sigma$, as mentioned above, the radius of the core particle is considered to be $\sigma_c-0.35\sigma$. Thus, σ_c essentially controls the radius of the core particle. Hereafter we call σ_c the core radius parameter. In the present study, we vary the core radius parameter σ_c within the range $1.40\sigma-1.90\sigma$, which roughly corresponds to 3.0–4.5 nm for the radius of the core particle (6.0–9.0 nm for the diameter). We will show that the size of the core particle is crucial for proper selection of the wrapping direction of the polymer.

B. Potential function for the coupling between bending and twisting

We next introduce the potential function $V_{\mathrm{bend,twist}}$ in Eq. (1). This function models the asymmetric coupling between the bending and twisting of DNA that is expected from the double-stranded helical structure. Instead of treating the double-stranded helical structure of DNA explicitly, we use here the bending angles and dihedral angles of our model polymer to incorporate the bending-twisting coupling at the coarse-grained level. We introduce the following two properties into our model polymer. (i) The polymer tends to twist in a particular direction upon bending. (ii) This tendency to twist becomes more significant as the polymer bends more.

We first define a "bending vector" $\boldsymbol{\nu}_i$ at each monomeric unit i as

$$\boldsymbol{\nu}_i = \boldsymbol{b}_{i-1} \times \boldsymbol{b}_i \quad (i = 2, \ldots, n-1), \tag{6}$$

where $\boldsymbol{b}_{i-1}$ and $\boldsymbol{b}_i$ are the bond vectors defined in Eq. (3) (see the schematic illustration in Fig. 1). We then introduce two parameters s_i and t_i that characterize the twisting of the polymer at bond i (the bond between monomer i and monomer $i+1$) as

$$s_i \equiv \frac{\boldsymbol{\nu}_i \cdot \boldsymbol{\nu}_{i+1}}{\sigma^4} = \frac{|\boldsymbol{\nu}_i||\boldsymbol{\nu}_{i+1}|}{\sigma^4}\cos\Phi_i \quad (i = 2, \ldots, n-2) \tag{7}$$

and

$$t_i \equiv \frac{(\boldsymbol{\nu}_i \times \boldsymbol{\nu}_{i+1})}{\sigma^4} \cdot \frac{\boldsymbol{b}_i}{|\boldsymbol{b}_i|} = \frac{|\boldsymbol{\nu}_i||\boldsymbol{\nu}_{i+1}|}{\sigma^4}\sin\Phi_i \quad (i = 2, \ldots, n-2), \tag{8}$$

where Φ_i is the dihedral angle between the plane spanned by the bond vectors $(\boldsymbol{b}_{i-1}, \boldsymbol{b}_i)$ and the plane spanned by $(\boldsymbol{b}_i, \boldsymbol{b}_{i+1})$,

$$\Phi_i \equiv \mathrm{sgn}[\boldsymbol{b}_i \cdot (\boldsymbol{\nu}_i \times \boldsymbol{\nu}_{i+1})]\cos^{-1}\left(\frac{\boldsymbol{\nu}_i \cdot \boldsymbol{\nu}_{i+1}}{|\boldsymbol{\nu}_i||\boldsymbol{\nu}_{i+1}|}\right) \quad (-\pi < \Phi_i \le \pi), \tag{9}$$

where $\mathrm{sgn}[\cdot]$ represents the sign of the scalar variable. The parameter s_i characterizes the degree of twisting at bond i, while the parameter t_i characterizes both the degree and the handedness (chirality) of the twisting. A positive sign of t_i corresponds to right-hand (clockwise) twisting of the polymer at bond i with respect to the *cis* conformation, while a negative sign of t_i corresponds to left-hand (counterclockwise) twisting.

By using the above twisting parameters $\{s_i\}$ and $\{t_i\}$ at respective bonds, we introduce the potential function for the coupling between bending and twisting as

$$V_{\text{bend,twist}} = \frac{\varepsilon}{2}\sum_{i=2}^{n-1} \kappa_i(s_{i-1}, s_i, t_{i-1}, t_i)\Theta_i^2, \tag{10}$$

where Θ_i is the bending angle between the vector $\boldsymbol{b}_{i-1}$ and the vector $\boldsymbol{b}_i$, which is defined as

$$\Theta_i \equiv \cos^{-1}\left(\frac{\boldsymbol{b}_{i-1}\cdot\boldsymbol{b}_i}{|\boldsymbol{b}_{i-1}||\boldsymbol{b}_i|}\right) \quad (0 \le \Theta_i \le \pi). \tag{11}$$

(See the schematic illustration in Fig. 1.) The parameter κ_i $(i=2,\ldots,n-1)$ in Eq. (10) acts as an effective spring constant for bending at bending site i (at monomeric unit i). However, in our model, κ_i is not a constant, but rather a function of the twisting parameters s_{i-1}, s_i, t_{i-1}, and t_i. The explicit functional form of κ_i is given by

$$\kappa_i = \kappa_0 - \kappa_{\text{bt}}[(\cos\Phi_0)(s_{i-1}+s_i) + (\sin\Phi_0)(t_{i-1}+t_i)], \tag{12}$$

where κ_0 is the spring constant that determines the intrinsic bending stiffness of the polymer at each bending site, while the constant κ_{bt} determines the strength of the coupling between bending and twisting. In the present model, these constants are set to be $\kappa_0=30$ and $\kappa_{\text{bt}}=12$, respectively. With these choices for κ_0 and κ_{bt}, the persistence length of the model polymer is roughly in the same order as the total length of the polymer and is much longer than the radius of the core particle, as in the case of real DNA and a nucleosome core. Thus, the model polymer is stiff enough so that it can wrap around the core particle in order. The parameter Φ_0 in Eq. (12) represents the "equilibrium dihedral angle," as explained below.

The physical meaning of Eq. (12) becomes clearer if one notes the following properties. Since the spring constant for bonding k_{bond} in Eq. (2) is large enough ($k_{\text{bond}}=400$) in our model, the distances between two neighboring monomeric units all remain close to the equilibrium distance; i.e., $b_i \simeq \sigma$ during the dynamics. Therefore, the magnitude of the vector $\boldsymbol{\nu}_i$ in Eq. (6) can be expressed approximately as $|\boldsymbol{\nu}_i| \simeq \sigma^2 \sin\Theta_i$. Insertion of this approximate equation into Eqs. (7) and (8) gives the following relationships:

$$s_i \simeq \sin\Theta_i \sin\Theta_{i+1} \cos\Phi_i, \tag{13}$$

$$t_i \simeq \sin\Theta_i \sin\Theta_{i+1} \sin\Phi_i. \tag{14}$$

Based on Eqs. (13) and (14), we can rewrite Eq. (12) as

$$\kappa_i \simeq \kappa_0 - \kappa_{\text{bt}}[\sin\Theta_{i-1}\sin\Theta_i\cos(\Phi_{i-1}-\Phi_0) + \sin\Theta_i\sin\Theta_{i+1}\cos(\Phi_i-\Phi_0)] \equiv \bar{\kappa}_i, \tag{15}$$

where we have introduced $\bar{\kappa}_i$ as an approximate expression for the original bending constant κ_i. Since $\sin\Theta_i$ (as well as $\sin\Theta_{i-1}$ and $\sin\Theta_{i+1}$) monotonically increases with Θ_i within the range $0 \le \Theta_i < \pi/2$, Eq. (15) indicates that the effect of the coupling between bending and twisting becomes stronger as the bending of the polymer at sites $(i-1,i,i+1)$ increases. [In our model, it is sufficient to consider only the range $0 \le \Theta_i < \pi/2$ for the bending angles since our DNA model is stiff (semiflexible) and the bending angles $\{\Theta_i\}$ do not exceed $\pi/2$ in our simulations.] As can be seen from Eq. (15), the condition $\Phi_{i-1}=\Phi_i=\Phi_0$ gives the minimum of $\bar{\kappa}_i$ for fixed values of Θ_{i-1}, Θ_i, and Θ_{i+1}. This is why Φ_0 can be regarded as the equilibrium dihedral angle.

To visually understand the above-mentioned basic properties of the bending-twisting elasticity of our model, we plotted the potential function

$$\bar{V}_{\text{bend,twist},i} = \frac{\varepsilon}{2}\bar{\kappa}_i(\Theta_{i-1},\Theta_i,\Theta_{i+1},\Phi_{i-1},\Phi_i)\Theta_i^2 \tag{16}$$

in Figs. 1(a)–1(f) for different conditions. Note that the potential function $\bar{V}_{\text{bend,twist},i}$ is a function of the five angular variables Θ_{i-1}, Θ_i, Θ_{i+1}, Φ_{i-1}, and Φ_i. In Figs. 1(a)–1(c), $\bar{V}_{\text{bend,twist},i}$ is plotted (with solid curves) as a function of Θ_i by fixing other angular variables to $\Theta_{i-1}=\Theta_{i+1}=\pi/6$ and $\Phi_{i-1}=\Phi_i=\Phi_0$ [in Fig. 1(a)], $\Phi_{i-1}=\Phi_i=\Phi_0\pm\pi/2$ [in Fig. 1(b)], and $\Phi_{i-1}=\Phi_i=\Phi_0\pm\pi$ [in Fig. 1(c)], respectively. For comparison, a normal harmonic potential $(\varepsilon/2)\kappa_0\Theta_i^2$ is plotted with dashed curves in Figs. 1(a)–1(c). From these figures, we see that the potential $\bar{V}_{\text{bend,twist},i}$ increases the most moderately with Θ_i if the nearby dihedral angles Φ_{i-1} and Φ_i are equal to the equilibrium value Φ_0 [Fig. 1(a)]. On the other hand, if the dihedral angles Φ_{i-1} and Φ_i are directed opposite the equilibrium direction—i.e., $\Phi_{i-1}=\Phi_i=\Phi_0\pm\pi$—the potential function $\bar{V}_{\text{bend,twist},i}$ increases the most steeply with Θ_i [Fig. 1(c)]. If $\Phi_{i-1}=\Phi_i=\Phi_0\pm\pi/2$ [Fig. 1(b)], the potential function $\bar{V}_{\text{bend,twist},i}$ coincides with the harmonic potential $(\varepsilon/2)\kappa_0\Theta_i^2$. In essence, the polymer can bend most easily at the bending site i if the polymer is twisted so that the two adjacent dihedral angles Φ_{i-1} and Φ_i are equal to the equilibrium value Φ_0.

The potential function $\bar{V}_{\text{bend,twist},i}$ in Eq. (16) can also be regarded as a function of the dihedral angles Φ_{i-1} and Φ_i by fixing the bending angles Θ_{i-1}, Θ_i, and Θ_{i+1}, as shown in Figs. 1(d)–1(f). In these figures, the equilibrium dihedral angle Φ_0 is set to $\Phi_0=-\pi/3$ as an example. If the polymer is not bent at the bending sites $i-1$, i, and $i+1$—i.e., $\Theta_{i-1}=\Theta_i=\Theta_{i+1}=0$—the potential surface for the dihedral angles Φ_{i-1} and Φ_i is flat and has no dependence on these dihedral angles [see Fig. 1(d)]. However, as the polymer bends to a greater extent at these bending sites, the dependence of $\bar{V}_{\text{bend,twist},i}$ on the dihedral angles Φ_{i-1} and Φ_i becomes more prominent [see Figs. 1(e) and 1(f)]. The elevation of the potential surface in these figures is due to the increase in the bending potential energy. In both Figs. 1(e) and 1(f), the minimum of the potential surface is located at the equilibrium point $(\Phi_{i-1},\Phi_i)=(\Phi_0,\Phi_0)$, while the maximum is located at $(\Phi_{i-1},\Phi_i)=(\Phi_0+\pi,\Phi_0+\pi)$. Thus, for fixed values of Θ_{i-1}, Θ_i, and Θ_{i+1}, the polymer tends to twist at bonds $i-1$ and i so that the corresponding dihedral angles Φ_{i-1} and Φ_i approach the equilibrium value $(\Phi_{i-1},\Phi_i)=(\Phi_0,\Phi_0)$. Note that this tendency to twist becomes stronger as the polymer bends more. This reflects the fact that the more the DNA bends, the more strongly a torque arises to twist the DNA. We expect that this is an intrinsic property of double-stranded DNA. If Φ_0 is positive in our model, the polymer tends to twist in a right-handed manner at each bond upon bending. On the other hand, if Φ_0 is negative, the polymer

tends to twist in a left-handed manner at each bond upon bending. In this way, we can introduce asymmetry between right-hand and left-hand twisting through the sign of the equilibrium dihedral angle Φ_0.

We now discuss the sign of Φ_0 for the proper modeling of real DNA. In our model, we assume that the DNA molecule has a tendency to twist *in a left-handed manner* upon bending. A possible reason for this assumption is that the double-stranded helix of DNA might have a tendency to unwind upon bending as was shown by Marko and Siggia [26]. Since the double-stranded helix of DNA (B-form DNA) is right-handed (clockwise), this unwinding of the double strand corresponds to the *left-handed twisting* of DNA around the central axis. Thus, we set the equilibrium dihedral angle Φ_0 to a negative value in our model. We specifically set the parameter Φ_0 to $-\pi/3$ [as in Figs. 1(e)–1(g)] so that the system possesses a clear tendency to twist in a left-handed manner at each bond upon bending.

Our assumption here might be intuitively acceptable. However, it should be noted that the changes in the dihedral angles of our model and the changes in the degree of twist of the double-stranded helical structure of real DNA are not exactly the same. This is because the dihedral angles of our model are coarse-grained degrees of freedom of DNA while the double-stranded helical structure of DNA should be associated with more microscopic degrees of freedom. We will discuss the correspondence between the dihedral angles and the twist of the double-stranded helical structure of DNA more in detail elsewhere [38] by using more microscopic models.

C. Langevin dynamics

In this study, the aqueous environment is simulated by underdamped Langevin dynamics. Basic equations of motion for the monomeric units of the polymer and for the core particle are given by

$$m\frac{d^2\boldsymbol{r}_i}{dt^2} = -\zeta\frac{d\boldsymbol{r}_i}{dt} - \boldsymbol{\nabla}_{\boldsymbol{r}_i}V + \boldsymbol{g}_i(t), \tag{17}$$

$$m_{\mathrm{c}}\frac{d^2\boldsymbol{r}_{\mathrm{c}}}{dt^2} = -\zeta_{\mathrm{c}}\frac{d\boldsymbol{r}_{\mathrm{c}}}{dt} - \boldsymbol{\nabla}_{\boldsymbol{r}_{\mathrm{c}}}V + \boldsymbol{g}_{\mathrm{c}}(t), \tag{18}$$

where m and m_{c} are the mass of the monomeric units of the polymer and the mass of the core particle, respectively. The parameters ζ and ζ_{c} are the friction coefficients for the monomers and the core, respectively. In this study, the ratio m_{c}/m and the ratio ζ_{c}/ζ are determined in terms of the effective radius of the monomeric units and that of the core particle as follows. Since the radius of the monomeric units is considered to be $\sigma_m/2$ and that of the core particle is considered to be $\sigma_{\mathrm{c}}-\sigma_m/2$ as discussed in Eqs. (4) and (5), the mass ratio is set to $m_{\mathrm{c}}/m=(\sigma_{\mathrm{c}}-\sigma_m/2)^3/(\sigma_m/2)^3$ by assuming that the masses are proportional to the volumes. Similarly, the ratio between the friction coefficients is determined by the Stokes law as $\zeta_{\mathrm{c}}/\zeta=(\sigma_{\mathrm{c}}-\sigma_m/2)/(\sigma_m/2)$. In Eqs. (17) and (18), $\boldsymbol{g}_i(t)$ and $\boldsymbol{g}_{\mathrm{c}}(t)$ are random forces that obey the fluctuation-dissipation theorem with a zero average,

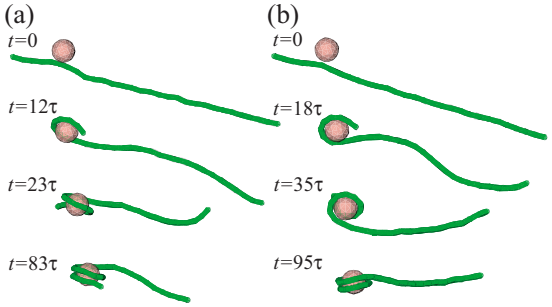

FIG. 2. (Color online) Two typical time evolutions of the model system forming a nucleosome. DNA is modeled by a semiflexible homopolymer and the histone core is modeled by a spherical particle. The size of the core is set at $\sigma_{\mathrm{c}}=1.6\sigma$. Time progresses from the top to the bottom in both (a) and (b) as indicated. In (a), the system achieves the proper left-handed wrapping, while in (b) the system undergoes improper right-handed wrapping.

$$\langle \boldsymbol{g}_i(t)\rangle = 0, \quad \langle \boldsymbol{g}_i(t)\boldsymbol{g}_j(t')\rangle = 6k_{\mathrm{B}}T\zeta\delta_{ij}\delta(t-t'), \tag{19}$$

$$\langle \boldsymbol{g}_{\mathrm{c}}(t)\rangle = 0, \quad \langle \boldsymbol{g}_{\mathrm{c}}(t)\boldsymbol{g}_{\mathrm{c}}(t')\rangle = 6k_{\mathrm{B}}T\zeta_{\mathrm{c}}\delta(t-t'), \tag{20}$$

where k_{B} is the Boltzmann constant and T is the temperature. δ_{ij} and $\delta(t-t')$ represent Kronecker's delta and delta function, respectively. After the following transformations of the variables in Eq. (17),

$$\boldsymbol{r}_i = \sigma\tilde{\boldsymbol{r}}_i, \quad t = \sqrt{\frac{m\sigma^2}{\varepsilon}}\tilde{t},$$

$$k_{\mathrm{B}}T = \varepsilon\tilde{T}, \quad \zeta = \sqrt{\frac{m\varepsilon}{\sigma^2}}\tilde{\zeta}, \tag{21}$$

and similar transformations in Eq. (18), where the variables with a tilde are dimensionless, the Langevin equations are transformed into dimensionless form. The velocity version of the Verlet algorithm [39] is used to solve the underdamped Langevin equations. The temperature is set to $k_{\mathrm{B}}T=0.5\varepsilon$ and the friction coefficient for the monomer is set to $\tilde{\zeta}=0.05$ in all computations in this study. Hereafter, numerical results are presented in scaled units; distances and positions are given in units of σ, and time and energy are given in units of $\sqrt{m\sigma^2/\varepsilon}\equiv\tau$ and ε, respectively.

III. WRAPPING DYNAMICS AND CHIRAL SELECTION

A. Wrapping of DNA around a core particle

Figure 2 exemplifies two different wrapping processes of the model DNA around a core particle. The initial conformation of the polymer is chosen randomly around a linear conformation. The size of the core is set to $\sigma_{\mathrm{c}}=1.6\sigma$ in both (a) and (b). In Fig. 2(a) (left column), the polymer achieves the proper left-handed wrapping, while in Fig. 2(b) (right column), the polymer "misfolds" into right-handed wrapping. We see that the polymer has created roughly 1.5–2 turns around the equator of the core particle in both Figs. 2(a) and 2(b). We have confirmed that, after the time evolution shown, the number of turns does not increase greatly in ei-

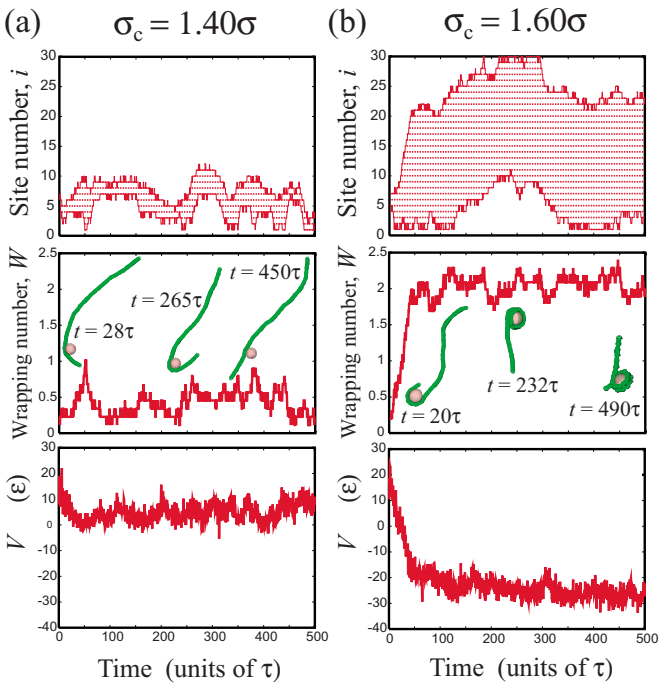

FIG. 3. (Color online) The two upper panels show typical time evolutions of adsorbed monomeric units of the polymer onto core particles with sizes (a) $\sigma_c=1.40\sigma$ and (b) $\sigma_c=1.60\sigma$. In each of these panels, the site numbers within the dotted region represent the adsorbed monomeric units at each time. The conformations of the system are shown in the two middle panels at the indicated times. The two middle panels show the corresponding time evolutions of the wrapping number W defined in Eq. (22). The two bottom panels show the corresponding time evolutions of the total potential energy V, Eq. (1), of the system (units of ϵ).

ther Fig. 2(a) or 2(b), but rather fluctuates roughly within the range 1–2.5. In addition, the core particle slips along the polymer under thermal fluctuations.

While the mechanism for the selection of the wrapping direction (chiral selection) is scrutinized in the next subsection, we focus here on the basic roles of the size of the core particle that are common to both left- and right-handed wrapping. The two upper panels in Fig. 3 show typical time evolutions of the site numbers of the adsorbed monomeric units of the polymer on a small core particle, $\sigma_c=1.40\sigma$, in (a), and on a large core particle, $\sigma_c=1.60\sigma$, in (b). In each of these panels, the site numbers in the dotted region represent the monomeric units that are adsorbed on the core particle at each time. Therefore, the vertical width of the dotted region represents the total number of adsorbed monomeric units at each time. Adsorption of a monomeric unit is judged depending on whether the distance between the monomeric unit and the center of the core particle is less than $\sigma_c+1.0\sigma$. In the top panel of (a), only a small number of monomeric units (about 1–10) are adsorbed on the core throughout the time duration. Thus, wrapping of the polymer around the core particle is incomplete in the time evolution in Fig. 3(a). For clarity, we show the corresponding conformations of the system at the three indicated times in the middle panel. In the time evolution in (b), the total number of adsorbed monomeric units increases rapidly in the first stage (from time $t=0$ to about $t=50\tau$), when the polymer wraps around the core in a left-handed manner as depicted in the middle panel. After this stage, the total number of adsorbed monomers does not change greatly, and instead, the position of the core particle slips along the polymer with time. The two middle panels in Fig. 3 show the corresponding time evolutions of the "wrapping number" W, which is defined as

$$W = \frac{\sigma(N_{\mathrm{ad}} - 1)}{2\pi\sigma_c}, \tag{22}$$

where N_{ad} is the total number of adsorbed monomeric units on the core particle. The numerator in Eq. (22) represents the length of the adsorbed part of the polymer on the core, while the denominator represents the length of a single turn of the polymer around the equator of the core. Since the polymer usually wraps around the equator in order, as shown in Fig. 2, the parameter W can be a good measure of the number of turns around the core. In (a), the wrapping number W rarely exceeds 1 and wrapping is incomplete, while in the time evolution in (b), the wrapping number W rapidly increases up to about 2 in the first stage, and after this stage, W fluctuates around 2. The two lowest panels in Fig. 3 show the corresponding time evolutions of the potential energy V of the whole system, Eq. (1). We see that V does not decrease sufficiently in the time evolution in (a), while in (b), V decreases markedly as wrapping progresses. This indicates that the wrapped state is energetically more stable than the unwrapped state in the case of a larger core particle in (b).

The above results in Fig. 3 indicate that the wrapping of the polymer around a smaller core is more difficult than wrapping around a larger core. This can be understood in terms of the competition between the bending energy of the polymer and the adsorption energy. When the polymer wraps around a small core, the polymer has to bend greatly at each monomeric site and, as a result, the energy cost for bending can exceed the stabilization effect due to adsorption of the polymer. Thus, wrapping around a small core is not preferred. On the other hand, the energy cost for bending can be small when the polymer wraps around a large core. Therefore, the system can wrap around a larger core more easily. This effect of core size is consistent with the experimental result by Zinchenko *et al.* [30], who showed that smaller core particles have to have larger positive charges for sufficient compaction of DNA to compensate for the energy cost of bending DNA. Correspondingly, in our model system, we confirmed that the parameter ε_c, which controls the strength of the interaction between the core and the monomers, has to be large for the system to achieve wrapping around a small core. Thus, it has become clear that a larger core particle is more advantageous for sufficient wrapping.

B. Chiral selection and order parameters

We next focus on the wrapping direction of DNA around a core particle—i.e., the chirality of such wrapping. The physical conditions for achieving the proper left-handed wrapping are highlighted. While the wrapping number W in Eq. (22) serves as a good order parameter to characterize the progress of wrapping, we introduce here another parameter C

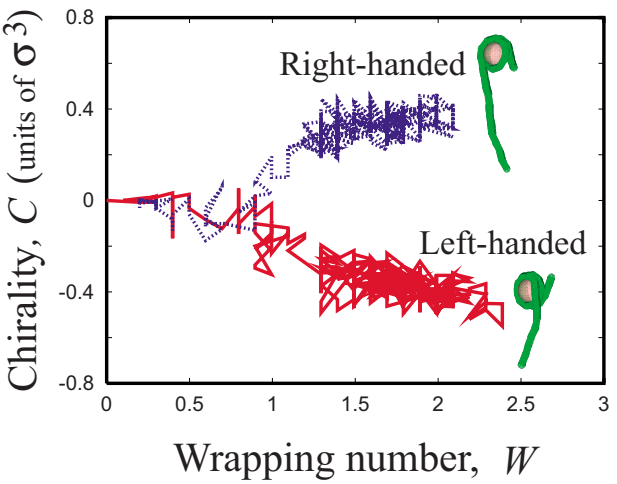

FIG. 4. (Color online) Two typical trajectories of the formation of a nucleosome projected onto the space of the two order parameters: wrapping number W and chirality parameter C. The solid trajectory corresponds to left-handed proper wrapping, while the dashed trajectory corresponds to right-handed improper wrapping. The size of the core is set to $\sigma_c = 1.60\sigma$ for the two trajectories.

that characterizes the chirality (handedness) of the wrapping, as follows. The N_{ad} adsorbed monomers on the core can be divided into the first $N_{ad}/2$ monomers (head group) and the last $N_{ad}/2$ monomers (tail group) depending on the monomer numbers. If N_{ad} is odd, we take $(N_{ad}-1)/2$ monomers for each group. In each of these groups, the average position of the monomers, $\langle \boldsymbol{r}_i \rangle_{head}$ or $\langle \boldsymbol{r}_i \rangle_{tail}$, is computed. The order parameter C, which we call the chirality parameter, is then defined as

$$C \equiv \langle \boldsymbol{\nu}_i \rangle \cdot (\langle \boldsymbol{r}_i \rangle_{tail} - \langle \boldsymbol{r}_i \rangle_{head}), \tag{23}$$

where $\langle \boldsymbol{\nu}_i \rangle$ is the average of the bending vectors $\boldsymbol{\nu}_i$ [Eq. (6)] among all the N_{ad} monomers adsorbed on the core particle. A positive sign of C signifies right-handed wrapping of the polymer while a negative sign of C signifies left-handed wrapping. The parameter C has the dimension of volume.

Figure 4 shows the projection of two typical trajectories onto the space of the two order parameters W and C. The trajectory shown with the solid line corresponds to proper left-handed wrapping while the dashed line corresponds to improper right-handed wrapping. We see that while the wrapping number W characterizes the progress of wrapping, the chirality parameter C characterizes the direction of wrapping. The trajectories in Fig. 4 are discrete along the horizontal axis because the wrapping number W contains the factor of the integer $(N_{ad}-1)$ [see Eq. (22)]. From Fig. 4, we see that the distinction between left-handed and right-handed wrapping becomes clear after the system has formed about $W=0.5-1$ turn(s). It is natural that the two trajectories are clearly separated in the region where W is greater than about 1 (turn). Thus, the two-dimensional space of W and C can serve as good reaction coordinates for the study of chiral selection in wrapping.

Using the coordinate system (W,C), we can now investigate how chiral selection is achieved. The three figures on the left in Fig. 5 show the probability distribution of the system in the two-dimensional space of W and C, $p(W,C)$, for three different core sizes: (a) $\sigma_c = 1.40\sigma$, (b) $\sigma_c = 1.50\sigma$, and (c) $\sigma_c = 1.60\sigma$. We used 30 trajectories, each of which has a time duration of 1000τ, to obtain the probability distribution for each core size. The initial configurations of the polymer are set randomly around a collinear configuration for all trajectories, and the initial positions of the core particle are also set randomly in the vicinity of the polymer. The three figures on the right in Fig. 5 show the corresponding effective free-energy surfaces $F(W,C)$, which are approximately computed as

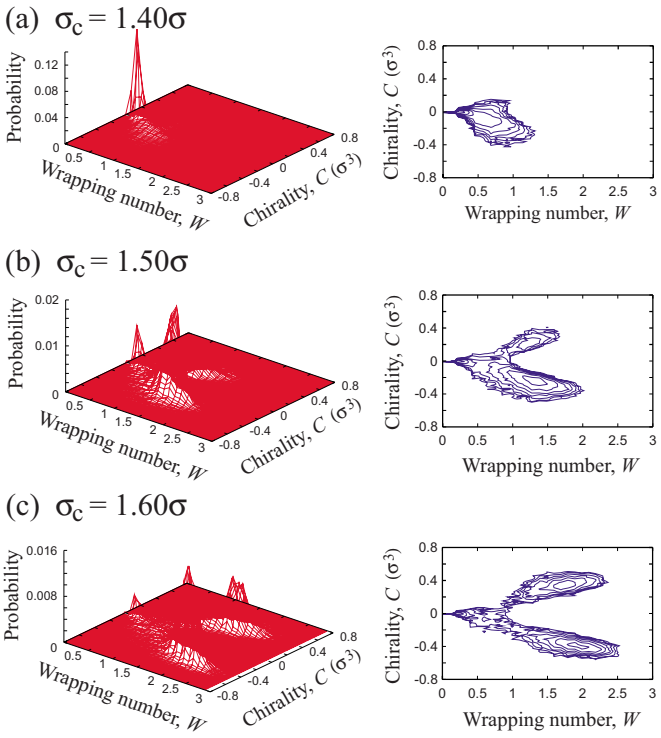

FIG. 5. (Color online) The three figures on the left show the probability distributions of the system in two-dimensional space of the wrapping number W and chirality parameter C (units of σ^3) for three different core sizes: (a) $\sigma_c = 1.40\sigma$, (b) $\sigma_c = 1.50\sigma$, and (c) $\sigma_c = 1.60\sigma$. The three figures on the right show the corresponding free-energy surfaces in the same space. The energy difference between two neighboring contour lines is 0.4ε.

$$F \simeq -k_B T \ln p(W,C). \tag{24}$$

The energy difference between two neighboring contour lines in the figures is 0.4ε.

For a small core, $\sigma_c = 1.40\sigma$ [Fig. 5(a)], the probability distribution has a single peak at around $(W,C)=(0.25,0)$, and correspondingly, the free-energy surface shows a well-like structure in this region. Since the peak of the probability distribution is located in the region where $W<1$, wrapping is generally not complete for a core of this size. This is consistent with the observations in Fig. 3(a). However, the probability distribution and the free-energy surface are biased toward the region where C is negative. This indicates that the

system tends to exhibit left-handed wrapping even though such wrapping is incomplete.

For a midsized core $\sigma_c=1.50\sigma$ [Fig. 5(b)], the topography of the probability distribution and that of the free-energy surface are quite different from those in Fig. 5(a). There are three peaks (wells) in the probability distribution (in the free-energy surface) for a core of this size. The heights of these three peaks are different. The highest peak is located in the region where C is negative and the wrapping number is about $W=1-2$. This peak corresponds to the left-handed wrapped state. A secondary peak occurs in the same region as in Fig. 5(a), which corresponds to the unwrapped state. There is a subtle peak in the region where C is positive and the wrapping number is about $W=1-1.5$. This subtle peak corresponds to the right-handed wrapped state. This result in Fig. 5(b) clearly shows that the system exclusively selects the left-handed wrapped state rather than the right-handed wrapped state for this intermediate core size. Correspondingly, the free-energy well of the left-handed wrapped state is much deeper and wider than that of the right-handed wrapped state. The fact that the wrapping number W in the right-handed wrapped state tends to be smaller than that in the left-handed wrapped state indicates that right-handed wrapping is indeed not very preferable. Thus, chiral selection is achieved for a core of this size.

The free-energy topography in Fig. 5(b) indicates that there are two kinds of transition states in this DNA-core complex system. The first is associated with the transition between the unwrapped and wrapped states (wrapping transition state), which is located around $(W,C)=(0.6,-0.1)$ in Fig. 5(b). The other is associated with the transition between the right-handed wrapped state and the left-handed wrapped state (chiral transition state), which is located around $(W,C)=(0.9,0.1)$. The fact that the value of W in the chiral transition state is greater than that in the wrapping transition state indicates that the system can switch the direction of wrapping without complete unwrapping of the polymer. Indeed, we have observed that the transition from the right-handed miswrapped state to the left-handed wrapped state occasionally takes place without complete unwrapping of the whole system. Thus, the distinction between the wrapping transition state and the chiral transition state should be important for the system to enhance the efficiency of chiral selection. This kind of conformational transition between the left- and right-handed wrapped states has also been observed experimentally [32].

For the large core, $\sigma_c=1.60\sigma$ [Fig. 5(c)], there are three peaks in the probability distribution, similar to Fig. 5(b): a peak that corresponds to the unwrapped state, a peak that corresponds to the left-handed wrapped state, and a peak that corresponds to the right-handed wrapped state. However, the main difference between Figs. 5(c) and 5(b) is that in the former the probabilities of the left-handed wrapped state and the right-handed wrapped state are similar. Therefore, chiral selection is not efficient for a large core even though the wrapping number W is large enough.

Figure 6 summarizes the results of Fig. 5 in terms of the one-dimensional free-energy curves along the chirality parameter C. In Fig. 6, the effective free energy is defined as $F/k_BT\equiv-\ln p(C)$, where $p(C)$ is the probability distribution

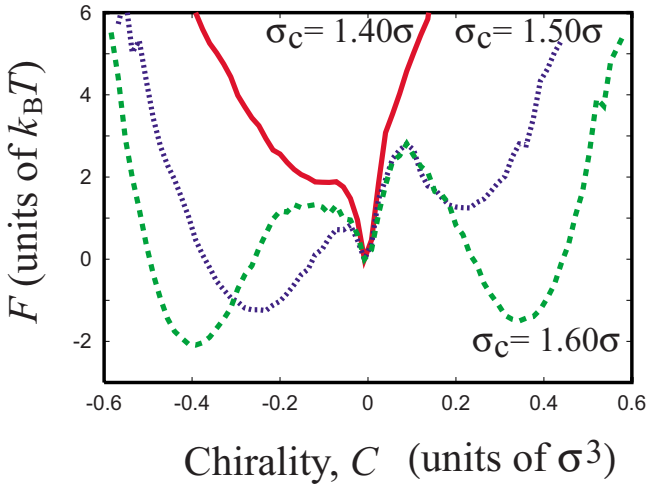

FIG. 6. (Color online) Free-energy profile of the system along chirality parameter C for three different core sizes. The solid, dotted, and dashed curves correspond to core sizes $\sigma_c=1.4\sigma$, $\sigma_c=1.5\sigma$, and $\sigma_c=1.6\sigma$, respectively.

of the system along the chirality parameter C. The probability $p(C)$ is obtained by integrating the distribution $p(W,C)$ in Fig. 5 with respect to W. For a small core, $\sigma_c=1.40\sigma$, the free-energy curve shows a single narrow and deep minimum at around $C=0$. This minimum corresponds to the unwrapped state. For the intermediate-size core, $\sigma_c=1.50\sigma$, the free-energy curve possesses two additional minima, which correspond to the left-handed wrapped state (on the left; $C<0$) and the right-handed wrapped state (on the right). For the intermediate-size core, $\sigma_c=1.50\sigma$, the free-energy curve is highly asymmetric with respect to the central line $C=0$. Thus, if the system is initiated in the vicinity of the unwrapped state ($C=0$), the system can easily surmount the low free-energy barrier (about $0.8k_BT$) to arrive at the deep minimum corresponding to the left-handed wrapped state. On the other hand, the system has to surmount a much higher free-energy barrier (about $2.8k_BT$) to enter the right-handed wrapped state. In addition, once the system is in the left-handed wrapped state, the system has to surmount a total free-energy barrier of about $4.0k_BT$ to enter the right-handed wrapped state. This asymmetric barrier structure secures the proper chiral selection for this intermediate-size core. When the core is larger, $\sigma_c=1.60\sigma$, the free-energy curve is relatively symmetric with respect to the central line $C=0$ and the probability of proper chiral selection is not high enough.

The results in Figs. 5 and 6 show that proper chiral selection is achieved with high accuracy if an appropriate size is selected for the core—e.g., $\sigma_c=1.50\sigma$. To explore the range of the appropriate core size, we computed relative probabilities of left-handed and right-handed wrapping. The results are shown in Fig. 7, where the relative percentages of the time spent in the left-handed wrapped state and the right-handed wrapped state are plotted as functions of the core-size parameter σ_c. To limit the time spent in states with an insufficient wrapping number from this computation, we counted only the time spent in the states where the wrapping number W is greater than 1.75 for both the left- and right-handed states. We used 100 trajectories, each of which has a

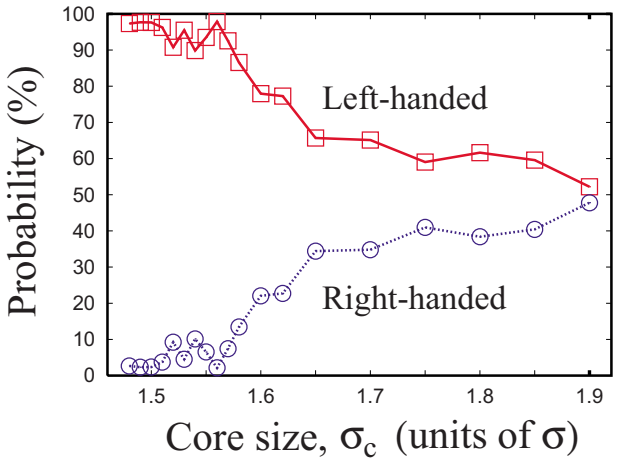

FIG. 7. (Color online) Dependence of the relative probabilities of the left-handed wrapped state (open squares) and the right-handed wrapped state (open circles) on the core radius parameter σ_c.

time duration of 500τ. The initial conditions of these trajectories were chosen randomly. The probability of the proper left-handed wrapping is not very high (50%–70%) for larger core sizes ($\sigma_c \geq 1.65\sigma$). However, as the core particle becomes smaller ($\sigma_c < 1.65\sigma$), the percentage of proper left-handed wrapping increases markedly. If the core size parameter σ_c is equal to 1.57σ or smaller, the system achieves the proper left-handed wrapping with an accuracy of more than 90%. If the core size parameter σ_c is smaller than 1.52σ, the accuracy tends to be more than about 95%. In reality, the accuracy of chiral selection may not necessarily be 100% under thermal fluctuations, especially at the single-nucleosome level. Indeed, it is experimentally observed [32] that the right-handed miswrapped state can arise under thermal fluctuations with a relatively high probability when the $(H3\text{-}H4)_2$ tetramer is used as a core particle.

Thus Fig. 7 clearly shows that a smaller core particle is more *advantageous* for achieving proper chiral selection in wrapping. However, if the core is too small, the polymer cannot wrap around the core for a sufficient number of turns because of the cost of the bending energy, as we have seen in Figs. 3(a) and 5(a). Indeed, in our model system, if the core size is smaller than $\sigma_c = 1.48\sigma$, the polymer seldom achieves wrapping with more than $W = 1.75$ turns. Therefore, the core size should be large enough so that DNA can wrap for a sufficient number of turns, and at the same time, the core size should be small enough so that chiral selection is achieved with high accuracy. Our results suggest that because of this trade-off between the wrapping number and the chiral selectivity, the range of appropriate core size is relatively narrow. In our model system, the appropriate core size should be about $\sigma_c = 1.48\sigma - 1.57\sigma$ in view of Fig. 7.

Finally, the ratio between the diameter of our model DNA and that of the core is consistent with a real system. In a real system, the radius of DNA is about 1 nm, while that of the core is about 3.3 nm. Therefore the radius of the core is 3.3 times larger than that of DNA. In our model system, the radius of DNA is roughly $\sigma_m/2 = 0.35\sigma$ and that of the core particle is $\sigma_c - \sigma_m/2$, which is equal to 1.15σ if σ_c is chosen to be 1.5σ. In this case, the ratio between the diameter of our model DNA and that of the core is also $1.15\sigma/0.35\sigma \approx 3.3$, which is consistent with the actual value.

C. Discussion: Energetics of chiral selection

We discuss here the reason why the probability of selecting the proper left-handed wrapping increases as the size of the core decreases. A qualitative explanation is as follows. When the polymer wraps around a small core, the polymer needs to bend largely. This large bending develops the tendency of the polymer to twist in a left-handed manner [see Figs. 1(d)–1(f)] and, in turn, the tendency of forming the left-handed superhelix around the core. On the other hand, if the core is large, the polymer does not need to bend largely upon wrapping and the tendency of twisting is not fully developed. As a result, for a large core, the left-handed and right-handed wrapping occur rather evenly.

To be more quantitative, we consider the bending-twisting energy of a single loop (turn) of a superhelix of our model DNA wrapped around a core particle. Let the radius of the loop be σ_c, which is the core radius parameter. Due to the self-avoiding effect, both ends of the loop do not match each other, but are separated in the direction of the central axis of the superhelix by the pitch distance σ_m, which is equal to twice of the radius of the model DNA. Because of this mismatch of the end points, we can define the handedness (chirality) of the loop. Let the total number of the monomeric units in the loop adsorbed on the core be N_{ad}. For simplicity, we assume that all the bending angles $\{\Theta_i\}$ and dihedral angles $\{\Phi_i\}$ in the loop are equal to $\bar{\Theta}$ and $\bar{\Phi}$, respectively. In addition, we assume that all the bond distances between two adjacent monomers are equal to the equilibrium value σ [cf. Eq. (3)]. By applying these assumptions to Eq. (12), the total bending-twisting potential energy of the single loop of DNA is estimated to be

$$V_{\text{bend,twist}}^{\text{loop}} = \frac{\varepsilon}{2}[\kappa_0 - 2\kappa_{\text{bt}} \sin^2 \bar{\Theta} \cos(\bar{\Phi} - \Phi_0)]\bar{\Theta}^2 N_{\text{ad}}. \tag{25}$$

To see the dependence of this bending-twisting energy $V_{\text{bend,twist}}^{\text{loop}}$ on the size of the core particle, we next express Eq. (25) as a function of the core radius parameter $\sigma_c/\sigma \equiv x$. The total number of the monomeric units in the loop, N_{ad}, is approximately expressed as

$$N_{\text{ad}} \simeq 2\pi\sigma_c/\sigma = 2\pi x. \tag{26}$$

The common value of the bending angles $\bar{\Theta}$ is expressed as

$$\bar{\Theta} \simeq 1/x, \tag{27}$$

while the common value of the dihedral angles $\bar{\Phi}$ is estimated to be

$$\bar{\Phi} \simeq \pm \sigma_m/4\pi\sigma x^2, \tag{28}$$

where the positive/negative sign corresponds to the right- and left-handed loops of DNA. By inserting Eqs. (26)–(28) into Eq. (25), we can express the total bending-twisting en-

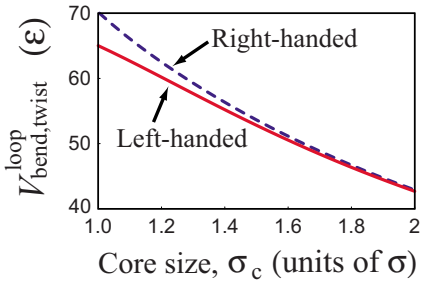

FIG. 8. (Color online) Bending-twisting potential energy $V^{\mathrm{loop}}_{\mathrm{bend,twist}}$ (units for ε) for a single loop of the model DNA plotted as a function of the core-radius parameter σ_c. The solid curve corresponds to the left-handed loop, while the dashed curve corresponds to the right-handed loop.

ergy of the DNA loop as a function of the core-radius parameter $x=\sigma_c/\sigma$:

$$V^{\mathrm{loop}}_{\mathrm{bend,twist}}(x) \simeq \frac{\pi\varepsilon\kappa_0}{x} - \frac{2\pi\varepsilon\kappa_{\mathrm{bt}}}{x}\sin^2\left(\frac{1}{x}\right)\cos\left(\pm\frac{\sigma_m}{4\pi\sigma x^2} - \Phi_0\right). \tag{29}$$

The first term on the right-hand side of Eq. (29) represents the bending energy of DNA, and the second term originates from the coupling between the bending and twisting. The second term makes the energy difference between the left-handed and right-handed loops.

Figure 8 shows the profile of $V^{\mathrm{loop}}_{\mathrm{bend,twist}}(\sigma_c/\sigma)$ in Eq. (29) for the left-handed (solid curve) and right-handed (dashed curve) loops. We see that as the size of the core decreases, the bending-twisting energy increases monotonically for both the left- and right-handed loops. This explains the fact that the wrapping around a small core is energetically more difficult than the wrapping around a large core due to the bending energy. It is also seen from Fig. 8 that the energy difference between the left-handed and right-handed loops becomes larger as the size of the core decreases. This explains the fact that the left-handed wrapping becomes energetically more favorable than the right-handed wrapping as the core becomes smaller. Thus the probability of selecting the proper left-handed wrapping increases as the size of the core decreases.

The energy difference between the left- and right-handed loops at $\sigma_c=1.5\sigma$ in Fig. 8 is about 0.82ε, which corresponds to $1.64k_BT$ in our simulation. This energy difference for a single loop of DNA corresponds to the energy difference of $2.87k_BT$ for the 1.75 turns in a regular nucleosome. This difference in the potential energy is comparable to the difference in the free energy between the left-handed and right-handed wrapped states in Fig. 6 at $\sigma_c=1.5\sigma$. Thus, we see that the chiral selectivity is primarily determined by the bending-twisting potential energy. The remaining important contribution to the chiral selection would be an entropic contribution: As can be seen from the free-energy surface in Fig. 5(b), the "wrapping pathway" from the unwrapped state to the left-handed wrapped state is much wider than that to the right-handed wrapped state. This makes the left-handed wrapped state more selectable. In this way, the difference in the width of the pathways should also contribute to the proper chiral selection.

IV. CONCLUDING REMARKS

By introducing a coarse-grained model for the formation of a nucleosome, we have shown that asymmetric coupling between the bending and twisting of DNA plays a predominant role in determining the direction of wrapping of DNA around a core particle. The basic assumption of our model is that DNA has a general tendency to twist in a left-handed manner upon bending, which is expected from the right-handed nature of the double-stranded helix of DNA. This bending-twisting coupling makes DNA select left-handed wrapping with high accuracy, provided that the size of the core is appropriate. If the core is too large, this chiral selection is not accurate enough. On the other hand, if the core is too small, DNA cannot wrap around the core for a sufficient number of turns. This is because the energy cost of bending exceeds the stabilization effect due to the adsorption of DNA on the core surface. If the core size is set within an appropriate range, DNA can select the proper left-handed wrapping with an accuracy of 90%–95%, or even higher. Our results suggest that nature has selected a histone core particle of the appropriate size so that the asymmetric nature of the coupling between bending and twisting of DNA can be effectively used in chiral selection in wrapping. It is expected that in chromatin, which has a poly-nucleosome structure, a cooperative effect [40] between neighboring nucleosomes will enhance the chiral selectivity to be 100%.

In the present study, the nucleosome core has been treated as a spherical particle since the main focus here has been on the role of the asymmetry (chirality) in the bending-twisting elasticity of DNA. However, in the real world, it is possible that the geometry of the core particle may also influence chiral selection. A real nucleosome core particle consists of two copies of four different proteins and has a disklike shape rather than a spherical shape [5]. It has been suggested [32,33] that a change in the topology of the core particle can induce a change in the handedness of wrapping of DNA. In addition, it is also known [2] that there are 14 regions on the core surface where wrapped DNA is adsorbed. These finer structures and the dynamics of the core particle may also guide the selection of chirality. In addition, in the real world, there may be a collective (or synergetic) effect among multiple nucleosomes: In chromatin, multiple nucleosomes are formed simultaneously and these interact with each other to form higher-order structures such as 30-nm fiber. These higher-order interactions among nucleosomes may also help to eliminate improper right-handed wrapping in nucleosomes. By considering these complementary effects, the accuracy of chiral selection in our present model is high enough at the single-nucleosome level.

The present study poses several intriguing issues for future study. As we have seen in the probability distributions and in the free-energy surfaces in Fig. 5, the wrapped state and the unwrapped state are separated by a barrier. This discontinuous nature of the wrapping transition may be a rem-

nant of the discontinuous coil-globule transition of a single DNA [11]. A recent experiment on chromatin reconstitution [40] has also suggested that DNA condensation induced by histone core particles is discontinuous. Thus, scrutiny of the fundamental properties of the wrapping-unwrapping transition of a nucleosome is of great importance. Another interesting issue is the transition between the left-handed wrapped state and the right-handed wrapped state of a nucleosome, which has been observed experimentally [32]. In the present model, we have found the distinction between the wrapping transition state and the chiral transition state in Fig. 5(b). This distinction might be of biological significance in the real nucleosome.

Finally, it would be a very important next step to clarify the correspondence between the finite number of degrees of freedom in our coarse-grained model and the extremely large number of degrees of freedom in the real DNA. The main focus of the present study has been the roles of the bending angles and dihedral angles of DNA, which are coarse-grained degrees of freedom. Therefore, it would be important to clarify the correspondence between these coarse-grained degrees of freedom and more microscopic degrees of freedom inherent in the real DNA. To this end, a comparison of the present model with more microscopic models that take into consideration the double-stranded helical structure explicitly would be quite useful [38]. Research toward this direction should further deepen our understanding of nucleosome dynamics.

ACKNOWLEDGMENTS

We would like to thank Dr. T. Sakaue, S. Araki, and Dr. T. Iwaki for their valuable discussions. In particular, discussions with Dr. T. Iwaki on DNA elasticity are gratefully acknowledged. We would also like to thank Professor K. Takeyasu and Dr. K. Hizume at Kyoto University for their kind comments. We are grateful to Professor D. Baigl for providing helpful comments.

[1] C. L. Woodcock and S. Dimitrov, Curr. Opin. Genet. Dev. **11**, 130 (2001).
[2] H. Schiessel, J. Phys.: Condens. Matter **15**, R699 (2003).
[3] G. J. Narlikar, H. Y. Fan, and R. E. Kingston, Cell **108**, 475 (2002).
[4] H. Zhou, Y. Zhang, Z. C. Ou-Yang, S. M. Lindsay, X. Z. Feng, P. Balagurumoorthy, and R. E. Harrington, J. Mol. Biol. **306**, 225 (2001).
[5] K. Luger, A. W. Mäder, R. K. Richmond, D. F. Sargent, and T. J. Richmond, Nature (London) **389**, 251 (1997).
[6] C. Bustamante, J. F. Marko, E. D. Siggia, and S. Smith, Science **265**, 1599 (1994).
[7] C. G. Baumann, V. A. Bloomfield, S. B. Smith, C. Bustamante, M. D. Wang, and S. M. Block, Biophys. J. **78**, 1965 (2000).
[8] M. Fixman and J. Kovac, J. Chem. Phys. **58**, 1564 (1973).
[9] M. Rubinstein and R. Colby, *Polymer Physics* (Oxford University Press, New York, 2003).
[10] L. D. Landau and E. M. Lifshitz, *Statistical Physics* (Pergamon, London, 1959).
[11] K. Yoshikawa, M. Takahashi, V. V. Vasilevskaya, and A. R. Khokhlov, Phys. Rev. Lett. **76**, 3029 (1996).
[12] H. Noguchi and K. Yoshikawa, J. Chem. Phys. **109**, 5070 (1998).
[13] H. Noguchi and K. Yoshikawa, J. Chem. Phys. **113**, 854 (2000).
[14] T. R. Strick, J.-F. Allemand, D. Bensimon, and V. Croquette, Biophys. J. **74**, 2016 (1998).
[15] J. F. Allemand, D. Bensimon, R. Lavery, and V. Croquette, Proc. Natl. Acad. Sci. U.S.A. **95**, 14152 (1998).
[16] S. Neukirch, Phys. Rev. Lett. **93**, 198107 (2004).
[17] T. Sakaue, K. Yoshikawa, S. H. Yoshimura, and K. Takeyasu, Phys. Rev. Lett. **87**, 078105 (2001).
[18] T. Sakaue and H. Löwen, Phys. Rev. E **70**, 021801 (2004).
[19] F. Robert, M. Douziech, D. Forget, J.-M. Egly, J. Greenblatt, Z. F. Burton, and B. Coulombe, Mol. Cell **2**, 341 (1998).
[20] G. Arya, Q. Zhang, and T. Schlick, Biophys. J. **91**, 133 (2006).
[21] J. Gore, Z. Bryant, M. Nöllmann, M. U. Le, N. R. Cozzarelli, and C. Bustamante, Nature (London) **442**, 836 (2006).
[22] T. Lionnet, S. Joubaud, R. Lavery, D. Bensimon, and V. Croquette, Phys. Rev. Lett. **96**, 178102 (2006).
[23] K. Besteman, S. Hage, N. H. Dekker, and S. G. Lemay, Phys. Rev. Lett. **98**, 058103 (2007).
[24] J. D. Moroz and P. Nelson, Proc. Natl. Acad. Sci. U.S.A. **94**, 14418 (1997).
[25] J. F. Marko, Europhys. Lett. **38**, 183 (1997).
[26] J. F. Marko and E. D. Siggia, Macromolecules **27**, 981 (1994).
[27] Z. Haijun and O. Y. Zhong-can, Phys. Rev. E **58**, 4816 (1998).
[28] P. J. Heath, J. B. Clendenning, B. S. Fujimoto, and J. M. Schurr, J. Mol. Biol. **260**, 718 (1996).
[29] M. Y. Tolstorukov, A. V. Colasanti, D. M. McCandlish, W. K. Olson, and V. B. Zhurkin, J. Mol. Biol. **371**, 725 (2007).
[30] A. A. Zinchenko, K. Yoshikawa, and D. Baigl, Phys. Rev. Lett. **95**, 228101 (2005).
[31] A. A. Zinchenko, T. Sakaue, S. Araki, K. Yoshikawa, and D. Baigl, J. Phys. Chem. B **111**, 3019 (2007).
[32] A. Hamiche, V. Carot, M. Alilat, F. De Lucia, M.-F. O'Donohue, B. Révet, and A. Prunell, Proc. Natl. Acad. Sci. U.S.A. **93**, 7588 (1996).
[33] W. Li, S.-X. Dou, and P.-Y. Wang, J. Theor. Biol. **235**, 365 (2005).
[34] S. Y. Park, R. F. Bruinsma, and W. M. Gelbart, Europhys. Lett. **46**, 454 (1999).
[35] E. M. Mateescu, C. Jeppesen, and P. Pincus, Europhys. Lett. **46**, 493 (1999).
[36] D. A. Beard and T. Schlick, Biopolymers **58**, 106 (2001).
[37] D. A. Heller, E. S. Jeng, T.-K. Yeung, B. M. Martinez, A. E. Moll, J. B. Gastala, and M. S. Strano, Science **311**, 508 (2006).
[38] T. Yanao and K. Yoshikawa (unpublished).
[39] Z. Guo and D. Thirumalai, J. Mol. Biol. **263**, 323 (1996).
[40] T. Nakai, K. Hizume, S. H. Yoshimura, K. Takeyasu, and K. Yoshikawa, Europhys. Lett. **69**, 1024 (2005).